Adiabatic and Nonadiabatic Reaction Pathways of the O(^{3}P) with Propyne

Shaolei Zhao, Weiqiang Wu, Hongmei Zhao, Huan Wang, Chunfan Yang, Kunhui Liu, and Hongmei Su*

State Key Laboratory of Molecular Reaction Dynamics, Beijing National Laboratory for Molecular Sciences (BNLMS), Institute of Chemistry, Chinese Academy of Sciences Beijing 100190, China

Received: August 25, 2008; Revised Manuscript Received: October 29, 2008

For the reaction of O(^{3}P) with propyne, the product channels and mechanisms are investigated both theoretically and experimentally. Theoretically, the CCSD(T)//B3LYP/6-311G(d,p) level of calculations are performed for both the triplet and singlet potential energy surfaces and the minimum energy crossing point between the two surfaces are located with the Newton−Lagrange method. The theoretical calculations show that the reaction occurs dominantly via the O-addition rather than the H-abstraction mechanism. The reaction starts with the O-addition to either of the triple bond carbon atoms forming triplet ketocarbene $^3CH_3CCHO$ or $^3CH_3COCH$ which can undergo decomposition, H-atom migration or intersystem crossing from which a variety of channels are open, including the adiabatic channels of CH_3CCO + H (CH_2CCHO + H), CH_3 + HCCO, CH_2CH + HCO, CH_2CO + CH_2, CH_3CH + CO, and the nonadiabatic channels of C_2H_4 + CO, C_2H_2 + H_2 + CO, H_2 + H_2CCCO. Experimentally, the CO channel is investigated with TR-FTIR emission spectroscopy. A complete detection of the CO product at each vibrationally excited level up to $v = 5$ is fulfilled, from which the vibrational energy disposal of CO is determined and found to consist with the statistical partition of the singlet C_2H_4 + CO channel, but not with the triplet CH_3CH + CO channel. In combination with the present calculation results, it is concluded that CO arises mainly from the singlet methylketene ($^1CH_3CHCO$) dissociation following the intersystem crossing of the triplet ketocarbene adduct ($^3CH_3CCHO$). Fast intersystem crossing via the minimum energy crossing point of the triplet and singlet surfaces is shown to play significant roles resulting into nonadiabatic pathways for this reaction. Moreover, other interesting questions are explored as to the site selectivity of O(^{3}P) atom being added to which carbon atom of the triple bond and different types of internal H-atom migrations including 1,2-H shift, 3,2-H shift, and 3,1-H shift involved in the reaction.

1. Introduction

The actual oxidation process of hydrocarbon fuels often involves the reactions of O(^{3}P) with unsaturated hydrocarbons including alkenes and alkynes. The reactions of O(^{3}P) with alkynes are therefore of importance in combustion. Also the addition reactions of the electrophilic oxygen atoms to the triple bond of alkynes serve as fascinating examples for chemical dynamics studies. The reaction of O(^{3}P) with alkynes has been attracting much attention of both experimental and theoretical studies.[1−22]

The reaction of O(^{3}P) with the simplest alkyne, C_2H_2, has been studied extensively. Experimental[1−12] and theoretical[13−15] studies agree that the primary products of O(^{3}P) + C_2H_2 reaction are produced mainly through two channels 1a and 1b. However, the potential H-atom abstraction channel, 1c, is negligible because of its large endothermicity of 31 kcal mol^{-1}.[5,12,15]

$$C_2H_2 + O(^3P) \rightarrow HCCO + H \quad \Delta H = -19 \text{ kcal mol}^{-1} \qquad (1a)$$

$$C_2H_2 + O(^3P) \rightarrow CH_2 + CO \quad \Delta H = -47 \text{ kcal mol}^{-1} \qquad (1b)$$

$$C_2H_2 + O(^3P) \rightarrow OH + CCH \quad \Delta H = +31 \text{ kcal mol}^{-1} \qquad (1c)$$

It has been well established that the major channel of the C_2H_2 + O(^{3}P) reaction is eq 1a, the HCCO + H channel.[1,3,5−7,9] Recent experiments[5−7,9] determined the yield of the HCCO + H channel to be about 80%, and the CH_2 + CO channel to be 15−20%. The calculation of Nguyen et al.[15] suggested that the HCCO + H yield is 93% at 300 K and drops to 90% at 1000 K, whereas the CH_2 + CO yield rises from 7% at 300 K to 10% at 1000 K. Their computation also shows that the HCCO + H yield dominates over the CH_2 + CO yield.

The mechanism of the O(^{3}P) + C_2H_2 reaction can be characterized as the electrophilic ground-state oxygen atoms being added to C−C triple bond,[12] forming a diradical intermediate HCCHO which is a ketocarbene initially. This diradical intermediate or its isomer, ketene CH_2CO formed via 1,2-H shift, can subsequently undergo unimolecular decomposition into HCCO + H (1a) or CH_2 + CO (1b), respectively. Recently, the potential energy surfaces for the C_2H_2 + O(^{3}P) reaction were theoretically investigated in detail.[15] Except for the two major channels presented above, the H-abstraction channel was calculated to have a high endothermicity (+31.9 kcal mol^{-1}) and thus cannot compete with the addition/elimination channels under any combustion conditions. In addition, an efficient reaction pathway on the electronically excited $^3A'$ surface resulting into H(^{2}S) + HCCO(A^2A') is predicted to play an important role at higher temperatures.

The reaction of O(^{3}P) with another important alkyne with the most similar structure to acetylene, propyne CH_3CCH, has also been studied previously. However, compared to the C_2H_2 + O(^{3}P) reaction, the studies are relatively scarce.[16−22] The total reaction rate constants at room temperature were determined to be at the magnitude of 10^{-13} cm^3 molecule^{-1} s^{-1}.[20−22]

* Corresponding author. E-mail: hongmei@iccas.ac.cn.

10.1021/jp8075707 CCC: $40.75
Published on Web 12/05/2008

In an early crossed molecular beam experiment, Kanofsky et al. observed seven reaction channels, including five major ones (2a–2e), for the reaction of CH_3CCH with $O(^3P)$.[17]

$$CH_3CCH + O(^3P) \rightarrow C_3H_3O + H \quad (2a)$$

$$CH_3CCH + O(^3P) \rightarrow C_2HO + CH_3 \quad (2b)$$

$$CH_3CCH + O(^3P) \rightarrow C_2H_4 + CO \quad (2c)$$

$$CH_3CCH + O(^3P) \rightarrow C_2H_2O + CH_2 \quad (2d)$$

$$CH_3CCH + O(^3P) \rightarrow C_2H_3 + HCO \quad (2e)$$

$$CH_3CCH + O(^3P) \rightarrow C_2H_2 + CO + H_2 \quad (2f)$$

$$CH_3CCH + O(^3P) \rightarrow C_3H_3 + OH \quad (2g)$$

Channels 2a and 2b are apparent displacement reactions and are analogous to the channel 1a in the $C_2H_2 + O(^3P)$ reaction, while channels 2c and 2f forming CO are analogous to 1b. It was believed that the first produced ethylidene radical CH_3CH, analogous to the product CH_2 in the $C_2H_2 + O(^3P)$ reaction, could either rearrange to yield ethylene or decompose to yield acetylene and H_2.[16,17,23] Another two major channels, the CH_2 channel (2d) and the HCO channel (2e), are new channels without analogy to the $O(^3P) + C_2H_2$ reaction. The H-abstraction channel forming OH, channel 2g, contributed just a small fraction for the total reaction. In order to determine the source of products of H, CH_3, HCO as well as OH, deuterated propyne CH_3CCD and CD_3CCH were, respectively, reacted with $O(^3P)$ to produce hydrogenated and deuterated products in their experiment.

In another more recent experiment by Bersohn et al. by means of LIF spectroscopy,[18] H, CO, and H_2 were observed as products from the reaction of $O(^3P)$ with propyne. The H and CO channels were determined to account for 48% yield of the total reaction. Moreover, possible mechanism was postulated based on the measurement of the product energy distribution. The CO product was found to be rotationally cold, from which they inferred that the initially formed triplet ketocarbene might cross to a singlet state and isomerize to a substituted ketene by a 1,2-H shift which then dissociated through a linear C−C−O transition state. The H_2 with $J \leq 3$ and rotational temperature of about 400 K was considered to be from the decomposition of CH_3CH or its isomer C_2H_4. In addition, H atoms have a lower translational energy for $O(^3P)$ + propyne reaction than that for the reaction of $O(^3P)$ with C_2H_2. They thought this is due to the presence of nine additional modes which effectively cool the remainder of the ketocarbene.

Evidently, previous experiments have shown that the product channels for the reaction of propyne with $O(^3P)$ are far more complex than its prototype reaction of acetylene with $O(^3P)$. The electrophilic $O(^3P)$ is added to the triple bond of alkyne forming a highly energized ketocarbene intermediate. It is expected that this high energy would allow direct decomposition or internal migration of H atoms before dissociation over even large barriers leading to a variety of open channels. The substitution of a methyl group to acetylene introduces additional degrees of freedom for the unimolecular decomposition and internal molecular rearrangements of the reaction intermediates. Thus, rich and complex product channels and reaction mechanisms are anticipated for the $O(^3P)$ + propyne reaction. To our best knowledge, no theoretical calculations have ever been performed for this reaction before.

In this work for the reaction system of $O(^3P)$ with propyne, the CCSD(T)//B3LYP/6-311G(d,p) level of theoretical calculations are performed for both the triplet and singlet potential energy surfaces and the minimum energy crossing point between the two surfaces are located with the Newton−Lagrange method. On the basis of the theoretical calculations the reaction channels and mechanisms are clarified. Interesting questions are explored as to the site selectivity of $O(^3P)$ atom being added to which carbon atom of the triple bond, different types of internal H-atom migrations including 1,2-H shift, 3,2-H shift, and 3,1-H shift involved in the reaction, and the nonadiabatic reaction pathways resulted from the intersystem crossing from triplet state to singlet state.

In addition to the theoretical calculation, experiments detecting the CO products are performed by means of step-scan time-resolved Fourier transform infrared emission spectroscopy (TR-FTIR). In the previous experiments by Bersohn et al.[18] with VUV LIF spectroscopy, CO was found to be almost entirely populated in the $v = 0$ vibrational ground state (the $v = 1/v = 0$ ratio of CO population was 0.05). It is obscure why CO was absent of vibrational energy despite the fact that the energy is initially localized on the newly formed C−O bond and the proposed pathway to produce C_2H_4 + CO on the singlet surface releases the largest amount of energy of 115.1 kcal mol^{-1} among all possible channels. In this work, by using TR-FTIR emission spectroscopy, a complete detection of the CO product at each vibrationally excited level is fulfilled, from which the vibrational energy disposal of CO is determined. The experiment shows that some vibrational energy, 6.2 kcal mol^{-1}, is released into the CO vibration with CO being vibrationally excited up to $v = 5$. The average vibrational energy is found to consist with the statistical partition of the singlet $C_2H_4(^1A)$ + CO channel, but not with the triplet CH_3CH + CO or $C_2H_4(^3A)$ + CO channel. In combination with the present calculation results, the CO product is identified to arise mainly from the singlet methylketene ($^1CH_3CHCO$) dissociation following the intersystem crossing of the triplet ketocarbene adduct ($^3CH_3CCHO$), i.e., the $C_2H_4(^1A)$ + CO channel. Fast intersystem crossing via the minimum energy crossing point of the triplet and singlet surfaces is shown to play significant roles resulting into nonadiabatic pathways for this reaction.

2. Computational and Experimental Methods

Computationally, the geometries of the reactants, products, various intermediates, and transition states are optimized using the hybrid density functional theory, i.e., Becke's three-parameter nonlocal exchange functional with the nonlocal correlation functional of Lee, Yang, Parr (B3LYP) with the standard 6-311G(d, p) basis sets.[24,25] For the current reaction involving eight atoms, the B3LYP/6-311G(d, p) level of theory is a balanced method considering the computational efficiency and accuracy. Harmonic vibrational frequencies and the zero-point energies (ZPE) are calculated at the same level with the optimized geometries. The intermediates are characterized by all the real frequencies. The transition states are confirmed by only one imaginary frequency. Connections of the transition states between two local minima have been confirmed by intrinsic reaction coordinate (IRC) calculations at the B3LYP/6-311G(d, p) level.[26] To obtain more reliable energetic data, single-point electronic energies are calculated at the CCSD(T)/6-311G(d, p) level using the B3LYP/6-311G(d, p) optimized geometries. All of the theoretical calculations are performed with the Gaussian 03 program package.[27] The minimum energy crossing point (MECP) on the intersection seam is located at the B3LYP/6-311G(d, p) level using the Newton−Lagrange method, which was introduced by Koga and Morokuma[28] to find the point where the energy is the lowest on the ($f - 1$)-dimensional hypersurface of seam between two f-dimensional potential energy surfaces. A homemade program is used for this purpose. This method has been applied successfully in locating the MECP for the reaction of O(^{3}P) with isobutene.[43]

Experimentally, the reaction products are monitored by step-scan, time-resolved Fourier transform emission (TR-FTIR) spectroscopy which is an effective technique probing IR-active reaction products in real time due to its multiplex advantage and nanosecond time resolution.[29] Step-scan FTIR spectrometer is commercially available but requires significant modification for coupling with pulsed laser to implement time-resolve IR spectral measurements. The details of the TR-FTIR spectrometer and the reaction chamber have been described previously.[30,31] Briefly, the instrument comprises a Nicolet Nexus 870 step-scan FTIR spectrometer, Spectra Physics (Quanta- Ray PRO 230) Nd:YAG laser, and a pulse generator (Stanford Research DG535) to initiate the laser pulse and achieve synchronization of the laser with data collection, two digitizers (internal 100KHz 16-bit digitizer and external 100 MHz 14-bit GAGE 8012A digitizer) which offer fast time resolution and a wide dynamic range as needed, and a personal computer to control the whole experiment. The detector used in this experiment is a liquid nitrogen cooled InSb detector.

The reaction is initiated in a stainless steel flow reaction chamber with a 20-L-volume. O(^{3}P) atoms were produced via the laser photodissociation of NO_2 at 355 nm (Nd:YAG laser, Spectra Physics Quanta-Ray PRO 230, pulse energy ~100 mJ). Only the ground-state O(^{3}P) atoms are produced following the 355 nm photolysis of NO_2 and there is no interference from O(^{1}D) atoms. Typically 200 mTorr of propynes (≥99.5%) and 150 mTorr of NO_2 (≥99.9%) without buffer gas enter the flow chamber 1 cm above the photolysis beam via needle valves. The chamber is pumped by an 8 L s^{-1} mechanical pump and the stagnation pressure of the chamber is measured by a MKS capacitance monometer. With the photolysis volume in the cylinder of 250 mL, it is expected that the flow rate is fast enough to replenish the sample at each laser pulse running normally at a repetition rate of 10 Hz.[30,31] The constant pressure of sample is maintained by adjusting the pumping speed and the needle valves. Transient infrared emission is collected by a pair of gold-coated White-Cell spherical mirrors and collimated by a CaF_2 lens to the step-scan FTIR spectrometer.

3. Results and Discussion

3.1. Theoretical Calculations of the Product Channels and Mechanisms. The optimized geometries of various reactants, intermediates, transition states and products at the B3LYP/6-311G(d,p) level are shown in Figure 1. The vibrational modes and imaginary frequencies of the transition states are also indicated. The zero-point vibrational energies at the B3LYP/6-311G(d,p) level, the single-point energies computed with the CCSD(T) method, and the relative energies by taking the energy of the reactants as zero are listed in Table 1. The energy difference between the reactants and products computed at the CCSD(T)//B3LYP/6-311G(d,p) level agrees well with the available experimental reaction enthalpies, demonstrating that the present level of calculation can provide reliable energetic and mechanistic information for the reaction of O(^{3}P) with propyne.

3.1.1. The Minimum Energy Crossing Point between the Singlet and Triplet States. The reaction starts on a triplet surface with the addition of O(^{3}P) to the triple bond of propyne forming a ketocarbene CH_3CCHO^* from which a variety of reaction channels are open. Also, previous experiments[17] indicated the existence of nonadiabatic pathways forming $C_2H_4 + CO$ after the initial triplet ketocarbene crosses to a singlet state. Therefore, reaction pathways on both triplet and singlet potential energy surfaces as well as the minimum energy crossing point (MECP) between the two states are calculated.

It has been shown that the characterization of the MECP[35−41] plays an important role in the investigation of the chemical reaction mechanism. For polyatomic molecules, there may be many intersections between two potential energy surfaces. The MECP on the intersection seam is very important and is usually considered as a "transition state" for the nonadiabatic process.

Koga and Morokuma[28] introduced the Newton−Lagrange method for the search of the MECP, which has the same geometry and energy for the singlet and triplet states. The energies, energy gradients, and Hessian matrixes of both singlet and triplet states are calculated, and the lowest-energy point is found on the seam of intersection at the B3LYP/6-311G(d,p) level. The obtained geometry for the MECP is between the two equilibrium geometries of ^{3}IM1 and ^{1}IM9 as shown in Figure 2. The energies and energy gradients of the MECP in the triplet and singlet states are listed in Table 2. The energy gradients of the MECP are not zero, unlike the optimization result of an equilibrium or a transition state geometry. The energy gradients of the MECP in the singlet state are proportional to that in the triplet state, and the ratio equals $-\lambda/(1 - \lambda)$, where λ is the Lagrange multiplier. These characteristics are shown to be reasonable, which is a good check for the obtained MECP.

The chemical reaction pathway can be found by the intrinsic reaction coordinate (IRC) method,[26] which is used to search the reaction paths of the intersystem crossing through the intersection. Figure 3 shows the minimum energy path from ^{3}IM1 to ^{1}IM9 through the MECP varying with the 2C−1C bond distance and 3C−1C−2C bond angle at the B3LYP/6-311G(d,p) level. The other coordinates are optimized. It can be seen that the MECP connects ^{3}IM1 and ^{1}IM9 properly. There is no experimental information about the energy barrier between ^{3}IM1 and the MECP. The calculations of this work show that this barrier is 13.9 kcal mol^{-1} above ^{3}IM1 at the CCSD(T)/6-311G(d,p) level. We will show later that the MECP plays a key role and the intersystem crossing has the lowest barrier among all reaction routes in the triplet state.

3.1.2. Adiabatic Pathways on the Triplet Potential Energy Surface. The adiabatic reaction pathways occurring on the triplet surface are explored and shown in Figure 4. The reaction starts with the addition of O(^{3}P) to either of the carbon atoms of the triple bond (the terminal carbon atom is referred to the C1 atom and the other is the C2 atom) or abstraction of an H atom from the methyl group. These three pathways are discussed separately and their relative importance is indicated based on the barrier height of the transition state (TS) as well as the rigidity of the TS, i.e., its "looser" or "tighter" entropic characteristic.

O-Atom Addition to the C1 Atom. Addition of the O atom to the C1 atom can occur via TS1 leading to the initial ketocarbene adduct IM1 (CH_3CCHO) lying 48.2 kcal mol^{-1} below the reactants. This step faces a barrier height of 5.4 kcal mol^{-1}. Starting from IM1, there are four different reaction pathways as follows: (i) breaking the C1−H bond to yield CH_3CCO + H atom via TS2 with a barrier of 38.9 kcal mol^{-1}; (ii) losing a methyl H atom via TS3 to form CH_2CCHO plus H atom, facing a barrier of 47.1 kcal mol^{-1}; (iii) isomerizing to IM2 (CH_3CHCO) by a 1,2-H shift via TS4 with a barrier of 44.5 kcal mol^{-1}; and (iv) rearranging to IM3 (CH_2CHCHO) via TS5 through a 3,2-H shift with a barrier of 46.7 kcal mol^{-1}. The

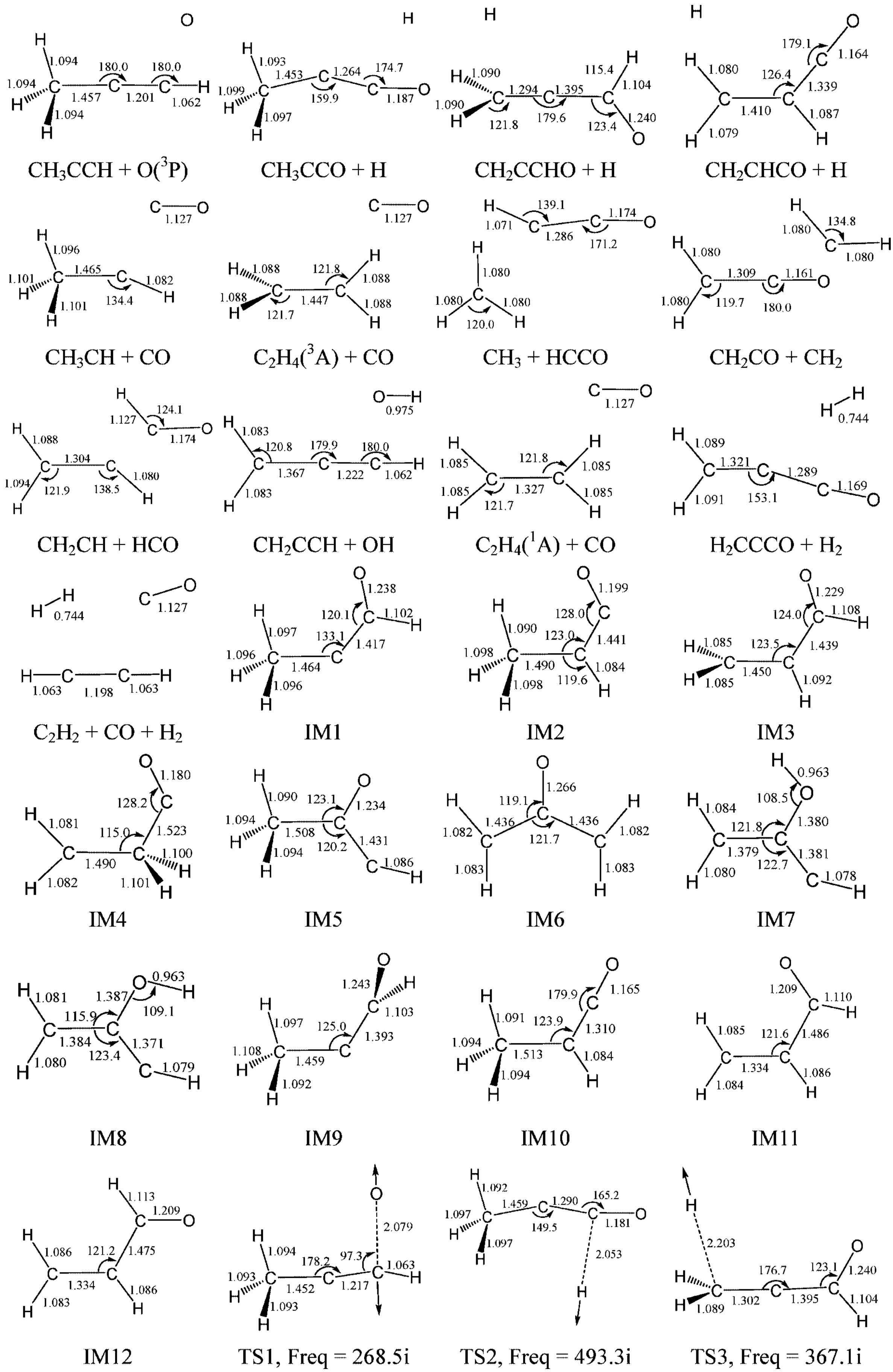

Figure 1. Part 1 of 2.

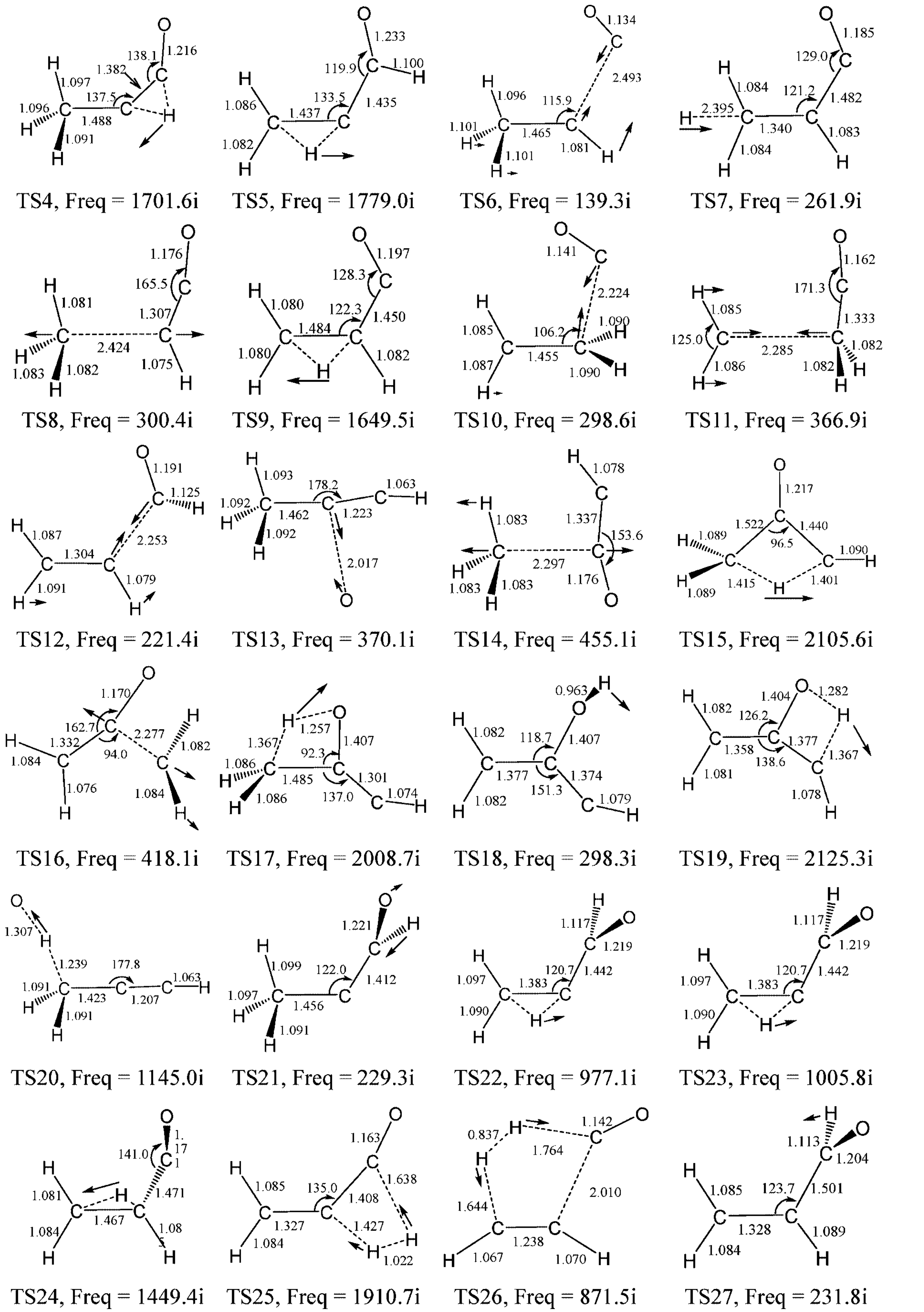

Figure 1. Part 2 of 2. Optimized geometries of reactants, intermediates, transition states, and products for the O(^{3}P) + CH_3CCH reaction at the B3LYP/6-311G(d, p) level. The vibrational modes and the imaginary frequencies of the transition states are also indicated. Bond lengths are in angstrom, bond angles are in degrees and imaginary frequencies are in cm^{-1}.

TABLE 1: Zero-Point Energies (ZPE, hartree), Total Energies (TE, hartree) and Relative Energies (RE, kcal mol^{-1}) Obtained by Taking the Energy of Reactants As Zero for Various Species in the O(^{3}P) + CH_3CCH Reaction

species	ZPE[a]	TE[b]	RE	ΔH_{298K}[c]	species	ZPE[a]	TE[b]	RE
C_3H_4 + O		−191.2371891	0.0		TS2(^{3}A)	0.049495	−191.2519642	−9.3
CH_3CCO + H		−191.2585157	−13.4		TS3(^{3}A)	0.047668	−191.2389389	−1.1
CH_2CCHO + H		−191.2437677	−4.1		TS4(^{3}A)	0.052819	−191.2430541	−3.7
CH_2CHCO + H		−191.2740194	−23.1		TS5(^{3}A)	0.053122	−191.2395944	−1.5
CH_3CH + CO		−191.3134707	−47.9		TS6(^{3}A)	0.052978	−191.3084379	−44.7
C_2H_4(^{3}A) + CO		−191.3200920	−52.0		TS7(^{3}A)	0.049455	−191.2696828	−20.4
CH_3 + HCCO		−191.2724856	−22.1	−26.4	TS8(^{3}A)	0.051801	−191.2609387	−14.9
CH_2CO + CH_2		−191.2683560	−19.6	−22.1	TS9(^{3}A)	0.054685	−191.2722334	−22.0
CH_2CH + HCO		−191.2674938	−19.0	−21.9	TS10(^{3}A)	0.053108	−191.3069492	−43.8
CH_2CCH + OH		−191.2442603	−4.4	−11.8	TS11(^{3}A)	0.051614	−191.2547985	−11.1
C_2H_4(^{1}A) + CO		−191.4206778	−115.1	−117.9	TS12(^{3}A)	0.052722	−191.2587638	−13.5
H_2CCCO + H_2		−191.3431980	−66.5		TS13(^{3}A)	0.055756	−191.2264549	6.7
C_2H_2 + CO + H_2		−191.3594572	−76.7	−76.0	TS14(^{3}A)	0.052590	−191.2584734	−13.4
IM1(^{3}A)	0.058492	−191.3139894	−48.2		TS15(^{3}A)	0.051747	−191.2501285	−8.1
IM2(^{3}A)	0.058962	−191.3400544	−64.5		TS16(^{3}A)	0.051536	−191.2528385	−9.8
IM3(^{3}A)	0.056508	−191.3174641	−50.4		TS17(^{3}A)	0.052029	−191.2151272	13.8
IM4(^{3}A)	0.056902	−191.3258612	−55.6		TS18(^{3}A)	0.056526	−191.2910346	−33.8
IM5(^{3}A)	0.057878	−191.3140792	−48.2		TS19(^{3}A)	0.050946	−191.2354739	1.1
IM6(^{3}A)	0.056900	−191.3317251	−59.3		TS20(^{3}A)	0.049691	−191.2186171	11.7
IM7(^{3}A)	0.057198	−191.2936118	−35.4		TS21(^{1}A)	0.056008	−191.3005295	−39.7
IM8(^{3}A)	0.057000	−191.2939019	−35.6		TS22(^{1}A)	0.055347	−191.2940147	−35.7
IM9(^{1}A)	0.057599	−191.3014430	−40.3		TS23(^{1}A)	0.055468	−191.2966087	−37.3
IM10(^{1}A)	0.060861	−191.4126978	−110.1		TS24(^{1}A)	0.055173	−191.2906739	−33.6
IM11(^{1}A)	0.061178	−191.4094665	−108.1		TS25(^{1}A)	0.049446	−191.2670007	−18.7
IM12(^{1}A)	0.061094	−191.4117219	−109.5		TS26(^{1}A)	0.048491	−191.2813782	−27.7
TS1(^{3}A)	0.055729	−191.2285956	5.4		TS27(^{1}A)	0.060042	−191.4009522	−102.8

[a] Calculated at the B3LYP/6-311G(d, p) levels of theory. [b] Calculated at the CCSD(T)/6-311G(d, p) levels of theory, including ZPE. [c] The experimental reaction enthalpies at 298 K (in kcal mol^{-1}). The formation enthalpies are taken from refs 32, 33 and 34.

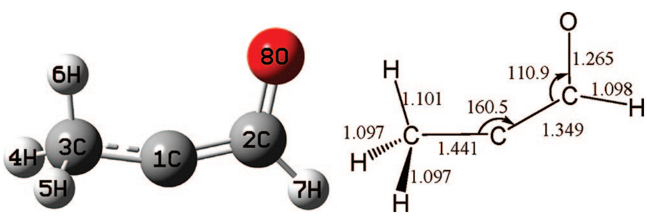

Figure 2. The optimized geometries and the numbering of atoms for the minimum energy crossing point (MECP) at the B3LYP/6-311G(d,p) level.

two H-atom displacement pathways, (i) and (ii), are more favorable than the two H-atom migration pathways, (iii) and (iv), due to the looser entropic character of the transition states.

The methylketene intermediate, IM2 (CH_3CHCO), lying 64.5 kcal mol^{-1} below the initial reactants, can decompose to triplet CH_3CH plus CO via TS6 by C1−C2 bond rupture, or to CH_2CHCO + H via TS7 by losing a H atom, or to CH_3 plus HCCO via TS8 by C2−C3 bond cleavage. These pathways confront barriers of 19.8 kcal mol^{-1}, 44.1 kcal mol^{-1} and 49.6 kcal mol^{-1}, respectively. In addition, IM2 can also isomerize to IM4 (CH_2CH_2CO) via TS9 with a barrier of 42.5 kcal mol^{-1}. Then IM4, 55.6 kcal mol^{-1} below the initial reactants, can either break C1−C2 bond to yield triplet C_2H_4 plus CO via TS10 overcoming a barrier of 11.8 kcal mol^{-1}, or decompose to ketene plus CH_2 via TS11 by C3−C2 bond rupture, facing a barrier of 44.5 kcal mol^{-1}. Among these four pathways starting from IM2, the decomposition channel to CH_3CH plus CO should be dominant, considering its lowest barrier height.

The aldehyde intermediate, IM3 (CH_2CHCHO), 50.4 kcal mol^{-1} below the initial reactants, can decompose to CH_2CH plus HCO via TS12 over a barrier of 36.9 kcal mol^{-1}.

O-Atom Addition to the C2 Atom. The addition of O(^{3}P) to C2 atom of the triple bond leads to another diradical adduct, IM5 (CH_3COCH), via TS13 after surmounting a barrier of 6.7 kcal mol^{-1}. This barrier is just a little higher than that of O-addition to C1 atom, indicating that the addition to C2 can somewhat compete with the addition to C1 atom. The identical binding energy of IM5 to IM1, 48.2 kcal mol^{-1}, also suggests that no preference is expected for the O(^{3}P) addition to either C1 or C2 atom. It can be concluded that there is no strong site selectivity when O(^{3}P) is added to the triple bond carbon atoms considering the nearly identical barrier height and binding energies of the adducts. Similar behavior of O(^{3}P) has also been observed experimentally[42] and verified later by theoretical calculations[43] when studying the reaction of O(^{3}P) with alkenes.

Starting from IM5 (CH_3COCH), there are three pathways, namely: (i) direct decomposition to CH_3 plus HCCO via TS14 with a barrier of 34.8 kcal mol^{-1}; (ii) isomerization to IM6 (CH_2COCH_2) by 3,1-H shift via TS15 overcoming a barrier of 40.1 kcal mol^{-1}, and then subsequent decomposition to ketene CH_2CO plus CH_2 via TS16 with a barrier of 49.5 kcal mol^{-1}; (iii) rearrangement to IM7 via TS17 with the subsequent isomerization and decomposition leading finally to CH_2CO + CH_2. Because TS17 lies 13.8 kcal mol^{-1} above the reactants, this reaction route is energetically unfavorable. No doubt, the CH_3 + HCCO channel is the most favorable of all the three pathways starting from the adduct IM5 (CH_3COCH). This can be explained by the fact that when oxygen atom being added to C2 atom, the weakest C3−C2 bond is subject to cleavage the most easily.

The H-Abstraction. The O(^{3}P) atom can abstract a methyl H atom in propyne via TS20 yielding hydroxyl OH plus propargyl radical CH_2CCH. Compared to the entrance barriers of O-addition reactions, TS20 is 6.3 and 5.0 kcal mol^{-1} higher in energy than TS1 and TS13, respectively. Consequently, the H-abstraction channel cannot compete with the O-addition channels. An alternate acetylenic H abstraction channel has been

TABLE 2: Energies (in Hartree) and Energy Gradients (g, in hartree/bohr) of the Minimum Energy Crossing Point (MECP) in the Triplet (T) and Singlet (S) States at the B3LYP/6-311G(d,p) Level[a]

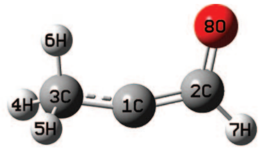

geometric parameters	MECP energy (S) -191.8533345 g(S)	MECP energy (T) -191.8533345 g(T)	g(S)/ g(T)
B1 (2C-1C)	0.00351	0.03471	0.101
B2 (3C-1C)	0.00054	0.00534	0.101
B3 (4H-3C)	-0.00013	-0.00125	0.104
B4 (5H-3C)	-0.00012	-0.00123	0.098
B5 (6H-3C)	0.00034	0.00332	0.102
B6 (7H-2C)	-0.00008	-0.00080	0.100
B7 (8O-2C)	0.00071	0.00698	0.102
A1 (3C-1C-2C)	-0.00253	-0.02492	0.102
A2 (4H-3C-1C)	-0.00056	-0.00557	0.101
A3 (5 H-3C-1C)	-0.00056	-0.00548	0.102
A4 (6 H-3C-1C)	0.00187	0.01853	0.101
A5 (7H-2C-1C)	0.00039	0.00394	0.099
A6 (8O-2C-1C)	0.00658	0.06500	0.101
D1 (4H-3C-1C-2C)	0.00071	0.00705	0.101
D2 (5H-3C-1C-2C)	-0.00073	-0.00716	0.102
D3 (6 H-3C-1C-2C)	0	0	
D4 (7H-2C-1C-3C)	0	0	
D5 (8O-2C-1C-3C)	0	0	

[a] Bond distances (B_n), angles (A_n), and dihedrals (D_n) are defined according to the numbering of the MECP in Figure 2.

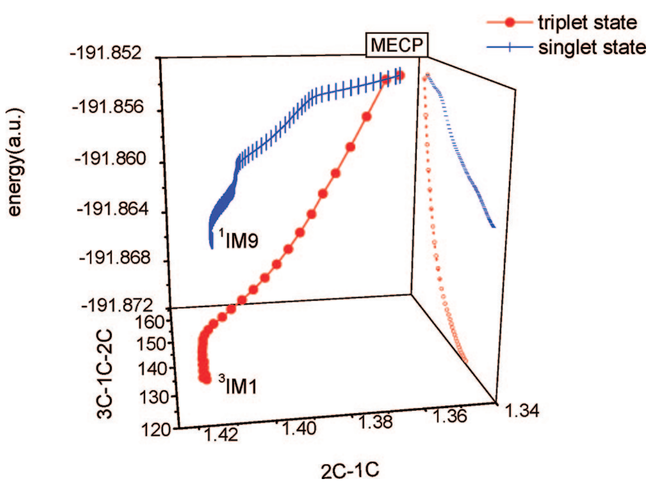

Figure 3. Minimum energy path from ^{3}IM1 to ^{1}IM9 through the minimum energy crossing point (MECP) varying with 2C−1C bond distance and 3C−1C−2C bond angle at the B3LYP/6-311G(d,p) level. (Other coordinates are optimized.)

ruled out since no transition state can be located for this type of H abstraction reaction.

Overall, the reaction on the triplet potential energy surface can be summarized by two types of reactions, i.e., H-abstraction and O-addition. The H-abstraction channels should contribute only a small fraction for the total reaction due to the high energy barrier (11.7 kcal mol^{-1}) it has to surmount. In contrast, the O-addition channels should account for most of the total reaction of O(^{3}P) with propyne and the addition can occur on both of the carbon atoms of the triple bond leading first to the diradical adducts IM1 (CH_3CCHO) and IM5 (CH_3COCH). Subsequently, the energized adducts IM1 and IM5 are subject to direct decomposition or H migrations (including 1,2-H shift, 3,2-H shift and 3,1-H shift) forming various isomeric intermediates IM2 (CH_3CHCO), IM3 (CH_2CHCHO), and IM6 (CH_2COCH_2), which decompose further to final products. Compared to the direct decomposition of the diradical adducts forming radical pairs CH_3CCO + H, CH_2CCHO + H and CH_3 + HCCO, the H migration channels forming eventually CH_2CH + HCO, CH_2CO + CH_2, C_2H_4(^{3}A) + CO and CH_3CH + CO are less competitive because the H migration requires surmounting higher barriers and more steps of molecular rearrangements. Also, the H and CH_3 displacement channels are further facilitated due to the looser entropic character of the direct decomposition. The most favorable reaction channels on the triplet surface are therefore concluded to be CH_3CCO + H (CH_2CCHO + H) and CH_3 + HCCO occurring via the direct decomposition of the diradical adducts IM1 and IM5. Interestingly, three types of H migrations are found to play equally important roles following the initial O-addition if considering their nearly identical barrier heights, i.e., 44.5 kcal mol^{-1} for the 1,2-H shift from IM1 to IM2, 46.7 kcal

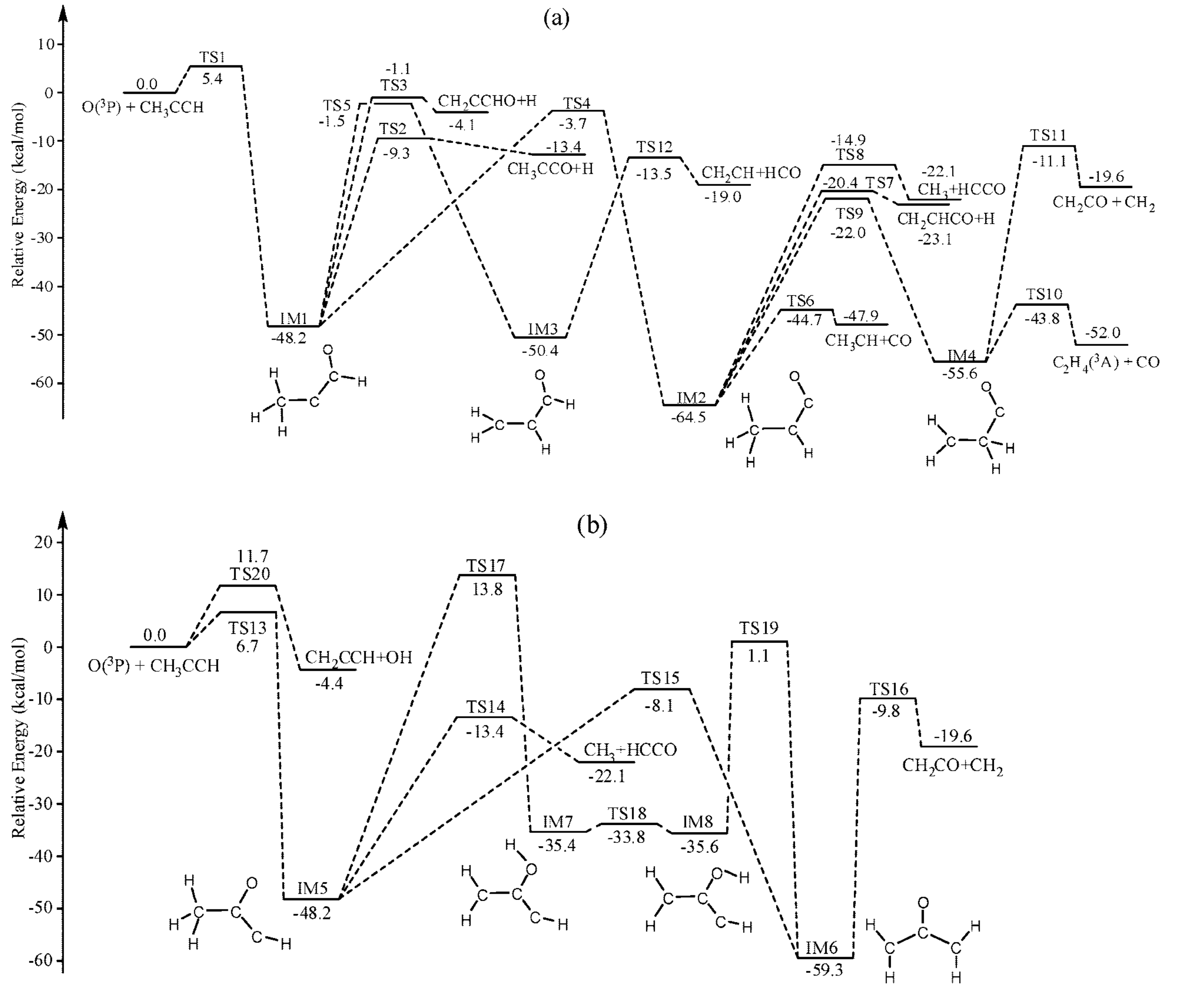

Figure 4. Potential energy profiles of the adiabatic reaction pathways on the triplet surface at the CCSD(T) //B3LYP/6-311G(d,p) level. Key: (a) reaction pathways starting from the O-atom addition to the C1 atom of the triple bond; (b) reaction pathways starting from the O-atom addition to the C2 atom of the triple bond; as well as the H-abstraction channel.

mol^{-1} for the 3,2-H shift from IM1 to IM3, and 40.1 kcal mol^{-1} for the 3,1-H shift from IM5 to IM6.

3.1.3. Nonadiabatic Pathways on the Singlet Potential Energy Surface. As discussed in section 3.1.1, the minimum energy crossing point between the triplet and singlet states has been located to be 13.9 kcal mol^{-1} above ^{3}IM1, and thus the intersystem crossing has the lowest energy barrier among the reaction routes of ^{3}IM1. Through MECP, the triplet ketocarbene ^{3}IM1 crosses into its singlet state ^{1}IM9 efficiently, from which a variety of nonadiabatic reaction pathways are open as shown in Figure 5.

On the singlet surface through a nearly barrierless 1,2-H shift process, ^{1}IM9 rearranges to the highly energized singlet methylketene, IM10, from which three channels are open: (i) cleaving the C1−C2 bond with the concerted 3,2-H shift via TS24 to yield $C_2H_4(^1A) + CO$; (ii) rearranging to IM12 which undergoes subsequently H_2 elimination while breaking the C1−C2 bond to yield ultimately $C_2H_2 + H_2 + CO$; (iii) subsequent rearrangement of IM12 to IM11 which undergoes H_2 elimination leading to $H_2 + H_2CCCO$. IM11 can also be formed via the 3,2-H shift of IM9 with a low barrier of 4.6 kcal mol^{-1}. The rate-limiting steps of the three channels, TS24 corresponding to the $C_2H_4(^1A) + CO$ channel, is the lowest in energy barrier compared to TS26 (corresponding to $C_2H_2 + H_2 + CO$ channel) and TS25 (corresponding to $H_2 + H_2CCCO$ channel). Therefore, the $C_2H_4(^1A) + CO$ channel dominates on the singlet surface and the $H_2 + H_2CCCO$ and $C_2H_2 + H_2 + CO$ are minor channels.

The nonadiabatic pathway of $C_2H_4(^1A) + CO$ via the singlet surface are far more exothermic ($\Delta H = -115.1$ kcal mol^{-1}) than that of the $CH_3CH + CO$ ($\Delta H = -47.9$ kcal mol^{-1}) and $C_2H_4(^3A) + CO$ ($\Delta H = -52.0$ kcal mol^{-1}) channels occurring on the triplet surface. In addition, the intersystem crossing through MECP corresponds to the lowest energy barrier among all the pathways of the ketocarbene ^{3}IM1 on the triplet surface. Therefore, CO is most likely produced from the singlet surface judging from the present theoretical calculation.

3.2. Experimental Investigation of the CO Channel. To assist identifying the source of CO produced whether from the triplet or singlet reaction pathways, the CO channel is probed by means of TR-FTIR emission spectra in the present experiment. This technique allows a complete detection of the product CO at each vibrationally excited level because it records the infrared fluorescence due to $v \rightarrow v - 1$ vibrational transitions of a whole set of vibrationally excited levels. Further spectral analysis can reveal an almost complete population distribution

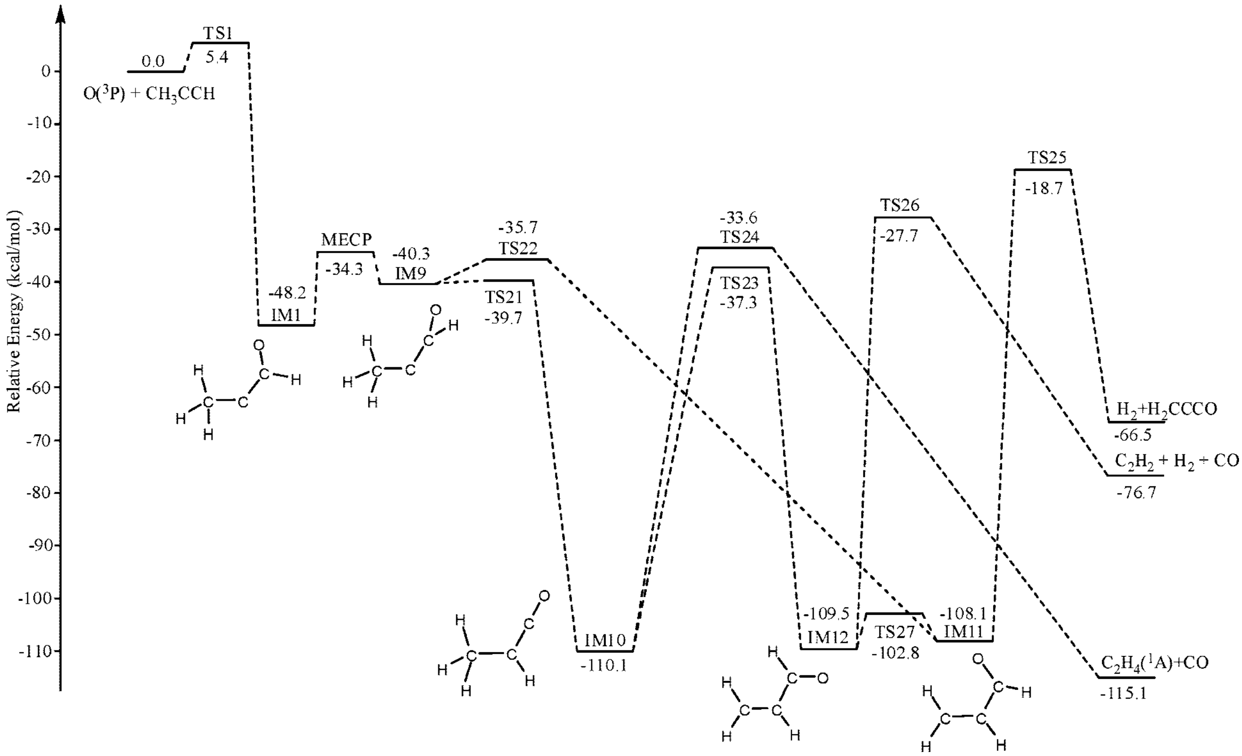

Figure 5. Potential energy profiles of the nonadiabatic reaction pathways on the singlet surface at the CCSD(T)//B3LYP/6-311G(d,p) level.

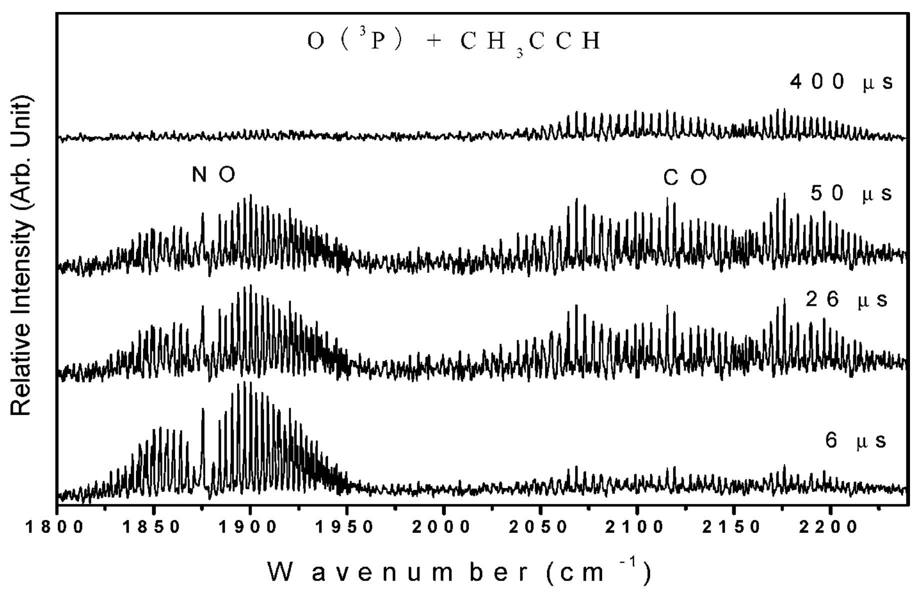

Figure 6. Product TR-FTIR emission spectra from the O(^{3}P) + CH_3CCH reaction taken at typical delay times from 6 to 400 μs after initiation of the reaction by 355 nm laser photolysis. The spectra were collected with a resolution of 0.5 cm^{-1}.

of vibrationally excited levels from which the product vibrational energy disposal can be determined.

In the first reference experiment, when pure propyne was irradiated by 355 nm laser, no IR emission was observed because propynes can not be photodissociated by a 355 nm laser. In the second reference experiment when pure NO_2 was irradiated by 355 nm laser, only the IR emission spanning from 1790 to 1970 cm^{-1} was observed due to the vibrationally excited photofragments of NO.

$$NO_2 + h\nu\ (355\ \text{nm}) \rightarrow NO + O(^3P)$$

Fortunately, the NO spectral region is isolated and will not interfere with the detection of the products of O(^{3}P) with propynes with the spectral region higher than 1970 cm^{-1}.

When the flowing gaseous mixture of O(^{3}P) precursor, NO_2, with propynes was irradiated by 355 nm laser, one rotationally resolved IR emission band spanning from 2000 to 2200 cm^{-1} was observed as shown in Figure 6. Judging from its spectral position and rotational structure, this band is assigned to the vibrationally excited CO products from the reaction of O(^{3}P) with propynes. The IR emission intensity of CO appears in a few microseconds and reaches its maximum intensity approximately at 50 μs.

A spectral fitting has been performed for the rotationally resolved CO emission bands using the spectral constants of CO and a nonlinear least-squares fitting program which has been described in detail elsewhere.[44] Representative fitting result for the 50 μs spectrum shown in Figure 7 a, demonstrates further

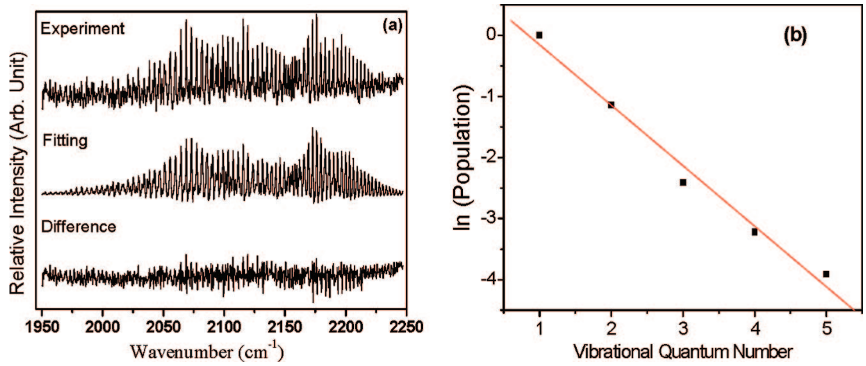

Figure 7. (a) Representative spectral fitting results for the IR emission bands of the product CO. (b) Representative Boltzmann plot of the vibrational distribution of CO. The straight line is the fit of the data to a Boltzmann distribution with a temperature of 3151 ± 223 K.

that this band is ascribed to CO. The best-fitted rotational temperature is nearly 300 K, the room temperature. This is reasonable because about 230 collisions take place within 50 μs at the total pressure of 350 mTorr with the rotational excitation of the products being quenched completely. To ensure adequate signal-to-noise ratios for detection purposes, the species partial pressures are necessarily relatively high, with which the rotational energy distribution is not possibly obtained because of collisions. The best fitted vibrational populations of CO are 1/0.32/0.09/0.04/0.02 for the vibrational levels of $\nu = 1-5$. The IR emission band of CO consists of five $\nu \rightarrow \nu - 1$ progressions of rovibrational transitions. As shown in Figure 7 b, the vibrational population can be fitted nicely by a Boltzmann distribution with a vibrational temperature of $T_{vib} = 3151 \pm 223$ K, corresponding to an average vibrational energy of 6.2 kcal mol^{-1}. This is presumably close to the nascent vibrational energy because of two reasons. First, with a reaction rate constant at the magnitude of 10^{-13} cm^3 molecule^{-1} s^{-1},[20−22] the products are still newly forming at 50 μs. Second, the vibrational distribution of CO is not expected to be altered much because the vibrational relaxation of CO is highly inefficient.[31] It shows here that some vibrational energy is released into the CO vibration. When probing CO with VUV LIF spectroscopy, Bersohn et al.[18] found that CO was populated almost entirely at $v = 0$ level and hence CO is lack of vibrational energy. This is somehow in conflict with the fact that the energy is initially localized on the newly formed C−O bond and the large exothermicity of 115.1 kcal mol^{-1} of the C_2H_4 + CO channel. As an absorption-based spectroscopy technique, LIF is probably not as sensitive as IR emission spectroscopy toward detecting molecules at vibrationally excited levels in some cases. This might be the reason why Bersohn et al. did not observe much CO at $v \geq 1$ levels.

The present theoretical calculation shows that there are two possible pathways producing CO either on the triplet or singlet surface:

$$CH_3CCH + O(^3P) \rightarrow CH_3CH + CO \text{ or } C_2H_4\,(^3A) + CO \quad \Delta H = -47.9 \text{ (or } -52.0) \text{ kcal mol}^{-1}$$

$$\rightarrow C_2H_4\,(^1A) + CO \quad \Delta H = -115.1 \text{ kcal mol}^{-1}$$

Considering the simplest possible statistical partition with the energy democratically released into the 13 vibrational and 3 relative translational modes of the C_2H_4 (^{1}A) + CO products on the singlet surface, the vibrational energy partitioned into CO should be 7.2 kcal mol^{-1}, while the triplet channels CH_3CH + CO and C_2H_4(^{3}A) + CO should yield CO with much less energy (3.0 or 3.2 kcal mol^{-1}). The average vibrational energy of 6.2 kcal mol^{-1} extracted from the CO IR emission spectra fits with the statistically predicted energy release from the singlet channel, but not with the triplet channels. This implies that CO should primarily arise from the singlet mechanism.

Interestingly, Bersohn et al.[18] observed that CO was also extremely cold in rotation and hence they speculated that CO was most likely produced from the decomposition of the singlet methylketene through a collinear C−C−O transition state to avoid torques on CO. Our calculation shows that the linear singlet methylketene (IM10) dissociates to form C_2H_4 (^{1}A) + CO through a transition state (TS24) with a bent C−C−O angle of 141^o. Although the calculation shows that the transition state leading to CO is not collinear as postulated,[18] the rotational excitation of CO should not to be large if produced from the slightly bent structure of TS24. Together with the CO vibrational energy disposal determined by the present experiment, it can now be concluded that CO arises mainly from the singlet methylketene ($^1CH_3CHCO$) dissociation following the intersystem crossing of the triplet ketocarbene adduct ($^3CH_3CCHO$). This is reasonable given the fact that the intersystem crossing via the minimum energy crossing point has the lowest barrier in all reaction routes of the triplet state $^3CH_3CCHO$ as shown in the theoretical calculation of this work. The minimum energy crossing point results into fast intersystem crossing, from which nonadiabatic reaction pathways such as C_2H_4 (^{1}A) + CO are open and play significant roles.

3.3. Comparison with Previous Experiments. Besides the above-discussed CO channel, the calculation reveals the formation mechanisms of a variety of other channels observed by previous crossed molecular beam or LIF experiments[17,18] as follows.

The H Channels. Our computational results show that H atom can be generated from three pathways: (i) the acetylenic H-atom displacement from IM1; (ii) the methyl H-atom displacement from IM1; (iii) the methyl H-atom displacement from IM2, the methylketene. Channel (i) producing acetylenic H-atom should dominate over channels (ii) and (iii) producing methyl H-atom because the former undergoes a much lower energy barrier, i.e., TS2 compared to TS3 and TS4. This prediction can explain nicely the previous experiments results. Kanofsky et al.[17] observed that the H/D ratios were about 0.1 and 10 for CH_3CCD and CD_3CCH as reactants with O(^{3}P), respectively. Beroshn et al.[18] obtained a H/D ratio of 0.770 ± 0.076 while determining the sources of H atoms with CH_3CCD as the reactant. Both experiments agree qualitatively that the acetylenic H-atom displacement is more advantageous over the methyl H-atom displacement.

The CH_3 Channels. Kanosfsky et al. determined the source of CH_3 product with CD_3CCH as a reactant, indicating that CH_3 is nearly all from the initial methyl group of propyne.[17] This is consistent with our computational results. The product CH_3 can be formed either from the direct displacement of CH_3 group from the C2-atom adduct IM5 via TS14 or from the displacement of CH_3 from triplet methylketene IM2 via TS8 following the 1,2-H shift of the C1-atom adduct IM1 via TS4. Certainly there is no exchange between methyl H and acetylentic H.

The HCO Channel and the CH_2 Channel. The calculation shows that HCO is formed on the triplet surface via the displacement of HCO moiety from IM3 following the rearrangement of IM1 (CH_3CCHO) to IM3 (CH_2CHCO) via a 3,2-H shift. While the most feasible pathway forming CH_2 is the isomerization of the C2-atom addition adducts IM5 (CH_3COCH) to IM6 (CH_2COCH_2) via a 3,1-H shift with the subsequent release of CH_2 and CH_2CO. These two channels occurring via the H-migration followed by decomposition are both energetically and kinetically accessible and thus should account for some major yields of the total reaction. The experimental measurement of Kanofsky et al.[17] also indicated these two to be among major channels. Furthermore, our calculation indicates that there is no H-atom exchange from methyl to acetylentic end when HCO is displaced from IM3, agreeing well with the observation[17] that DCO yield had a remarkable advantage over HCO yield for the reaction of O(^{3}P) with CH_3CCD.

To interpret the observation of the $CH_2CO + CH_2$ channel, Kanofsky suggested a possible mechanism via two steps of H shifts: $O + CH_3CCH \rightarrow CH_3C(O)CH \rightarrow CH_2(OH)CH \rightarrow CH_2C(O)CH_2 \rightarrow CH_2CO + CH_2$.[17] In order to validate the feasibility of this route, we also calculated the corresponding pathway, IM5 → TS17 → IM7 → TS18 → IM8 → TS19 → IM6 → TS16 → $CH_2CO + CH_2$. As shown in Figure 4 (b), this route turns out to be energetically inaccessible because it involves surmounting TS17 with the energy barrier 13.8 kcal mol^{-1} above the reactants. Instead, another feasible pathway via 3,1-H shift of IM5 (CH_3COCH) to IM6 (CH_2COCH_2) and the subsequent decomposition of IM6 is revealed in our calculation.

4. Conclusions

In brief, the product channels and mechanisms of the O(^{3}P) + CH_3CCH reaction are investigated both theoretically and experimentally. Theoretically, both of the reaction pathways on the triplet and singlet potential energy surfaces are calculated at the level of CCSD(T)//B3LYP/6-311G(d,p) and the minimum energy crossing point between the two surfaces are located with the Newton−Lagrange method. The theoretical calculations show that the reaction occurs dominantly via the O-addition rather than H-abstraction mechanism. The reaction starts with the O-addition to either of the triple bond carbon atoms forming triplet ketocarbene $^3CH_3CCHO$ or $^3CH_3COCH$ which can undergo decomposition, H-atom migration or intersystem crossing from which a variety of reaction channels become accessible, including the adiabatic channels of $CH_3CCO + H$ ($CH_2CCHO + H$), $CH_3 + HCCO$, $CH_2CH + HCO$, $CH_2CO + CH_2$, $CH_3CH + CO$, and the nonadiabatic channels of $C_2H_4 + CO$, $C_2H_2 + H_2 + CO$, and $H_2 + H_2CCCO$.

Experimentally with TR-FTIR emission spectroscopy, a complete detection of the vibrationally excited product CO up to $v = 5$ reveals that the energy released into the CO vibration (i.e., 6.2 kcal mol^{-1}) consists with the statistical partition of the singlet $C_2H_4(^1A) + CO$ channel, but not with the triplet $CH_3CH + CO$ or $C_2H_4(^3A) + CO$ channel. In combination with the present calculation results, it is concluded that CO arises mainly from the singlet methylketene ($^1CH_3CHCO$) dissociation following the intersystem crossing of the triplet ketocarbene adduct ($^3CH_3CCHO$). Fast intersystem crossing via the minimum energy crossing point of the triplet and singlet surfaces is shown to play significant roles resulting into nonadiabatic pathways for this reaction. The minimum energy crossing point is located to be 13.9 kcal mol^{-1} above the triplet $^3CH_3CCHO$, corresponding to the lowest energy barrier among all pathways on the triplet surface.

Overall, the initially formed O-addition ketocarbene adducts CH_3CCHO^* or CH_3COCH^* exhibits full scope of unimolecular decomposition and internal H-atom migration for the O(^{3}P) + CH_3CCH reaction. The addition of the O(^{3}P) to either of the carbon atoms of the triple bond is predicted to have almost equal chances because of the nearly identical barrier heights. Following the initial O-addition, three types of H-atom migrations including 1,2-H shift, 3,2-H shift, and 3,1-H shift are found to play equally important roles, from which additional channels become accessible.

Acknowledgment. This work is financially supported by the National Natural Science Foundation of China (Grant No. 20733005 and No. 20673126), the National Basic Research Program of China (2007CB815200, 2007AA02Z116) and the Chinese Academy of Sciences.

References and Notes

(1) Peeters, J.; Schaekers, M.; Vinckier, C. *J. Phys. Chem.* **1986**, *90*, 6552.
(2) Mahmud, K.; Fontijn, A. *J. Phys. Chem.* **1987**, *91*, 1918.
(3) Schmoltner, A. M.; Chu, P. M.; Lee, Y. T. *J. Chem. Phys.* **1989**, *91*, 5365.
(4) Peeters, J.; Vanhaelemeersch, S.; Van Hoeymissen, J.; Borms, R.; Vermeylen, D. *J. Phys. Chem.* **1989**, *93*, 3892.
(5) Michael, J. V.; Wagner, A. F. *J. Phys. Chem.* **1990**, *94*, 2453, and references therein.
(6) Boullart, W.; Peeters, J. *J. Phys. Chem.* **1992**, *96*, 9810.
(7) Peeters, J.; Boullart, W.; Langhans, I. *Int. J. Chem. Kinet* **1994**, *26*, 869.
(8) Huang, X.; Xing, G.; Bersohn, R. *J. Chem. Phys.* **1994**, *101*, 5818.
(9) Capozza, G.; Segoloni, E.; Leonori, F.; Volpi, G. G.; Casavecchia, P. *J. Chem. Phys.* **2004**, *120*, 4557.
(10) Chikan, V.; Leone, S. R. *J. Phys. Chem. A* **2005**, *109*, 2525.
(11) Arrington, C. A.; Brennan, W.; Glass, G. P.; Michael, J. V.; Niki, H. *J. Chem. Phys.* **1965**, *43*, 525.
(12) Cvetanovic, R. *Adv. Photochem.* **1963**, *1*, 115.
(13) Harding, L. B. *J. Phys. Chem.* **1981**, *85*, 10.
(14) Harding, L. B.; Wagner, A. F. *J. Phys. Chem.* **1986**, *90*, 2974.
(15) Nguyen, T. L.; Vereecken, L.; Peeters, J. *J. Phys. Chem. A* **2006**, *110*, 6696.
(16) Brown, J. M.; Thrush, B. A. *Trans. Faraday Soc.* **1967**, *63*, 630.
(17) Kanofsky, J. R.; Lucas, D.; Pruss, F.; Gutman, D. *J. Phys. Chem.* **1974**, *78*, 311.
(18) Xing, G.; Wang, X.; Bersohn, R. *J. Chem. Phys.* **1996**, *105*, 488.
(19) Herbrechtsmeier, P.; Wagner, H. Gg. *Z. Phys. Chem. Neue Folge* **1974**, *93*, 143.
(20) Arrington, C. A.; Cox, D. J. *J. Phys. Chem.* **1975**, *79*, 2584.
(21) Aleksandrov, E. N.; Dubrovina, I. V.; Kozlov, S. N. *Kinet. Catal. (Engl. Transl.)* **1981**, *22*, 394.
(22) Adusei, G. Y.; Blue, A. S.; Fontijn, A. *J. Phys. Chem.* **1996**, *100*, 16921.
(23) Jensen, J. H.; Morokuma, K.; Gordon, M. S. *J. Chem. Phys.* **1994**, *100*, 1981.
(24) Becke, A. D. *J. Chem. Phys.* **1993**, *98*, 5648.
(25) Lee, C.; Yang, W.; Parr, R. G. *Phys. Rev. B: Condens. Matter Mater. Phys.* **1988**, *37*, 785.
(26) Gonzalez, C.; Schlegel, H. B. *J. Phys. Chem.* **1990**, *94*, 5523.
(27) Frisch, M. J.; Trucks, G. W.; Schlegel, H. B.; Scuseria, G. E.; Robb, M. A.; Cheeseman, J. R.; Montgomery J. A., Jr.; Vreven, T.; Kudin, K. N.; Burant, J. C.; Millam, J. M.; Iyengar, S. S.; Tomasi, J.; Barone, V.; Mennucci, B.; Cossi, M.; Scalmani, G.; Rega, N.; Petersson, G. A.; Nakatsuji, H.; Hada,

M.; Ehara, M.; Toyota, K.; Fukuda, R.; Hasegawa, J.; Ishida, M.; Nakajima, T.; Honda, Y.; Kitao, O.; Nakai, H.; Klene, M.; Li, X.; Knox, J. E.; Hratchian, H. P.; Cross, J. B.; Bakken, V.; Adamo, C.; Jaramillo, J.; Gomperts, R.; Stratmann, R. E.; Yazyev, O.; Austin, A. J.; Cammi, R.; Pomelli, C.; Ochterski, J. W.; Ayala, P. Y.; Morokuma, K.; Voth, G. A.; Salvador, P.; Dannenberg, J. J.; Zakrzewski, V. G.; Dapprich, S.; Daniels, A. D.; Strain, M. C.; Farkas, O.; Malick, D. K.; Rabuck, A. D.; Raghavachari, K.; Foresman, J. B.; Ortiz, J. V.; Cui, Q.; Baboul, A. G.; Clifford, S.; Cioslowski, J.; Stefanov, B. B.; Liu, G.; Liashenko, A.; Piskorz, P.; Komaromi, I.; Martin, R. L.; Fox, D. J.; Keith, T.; Al.Laham, M. A.; Peng, C. Y.; Nanayakkara, A.; Challacombe, M.; Gill, P. M. W.; Johnson, B.; Chen, W.; Wong, M. W.; Gonzalez, C.; Pople, J. A. Gaussian, Inc.: Wallingford, CT, 2004.

(28) Koga, N.; Morokuma, K. *Chem. Phys. Lett.* **1985**, *119*, 371.

(29) Pibel, C. D.; Sirota, E.; Brenner, J.; Dai, H. L. *J. Chem. Phys.* **1998**, *108*, 1297.

(30) Zhu, Q. H.; Huang, S. L.; Wang, X. B.; Hao, Z.; Zhang, Q. F.; Cao, J. R.; Wu, X. J.; Lv, N.; Yao, S. X.; Kong, F. A. *Chin. J. Chem. Phys* **1993**, *6*, 87.

(31) Su, H. M.; Zhao, S. L.; Liu, K. H.; Xiang, T. C. *J. Phys. Chem. A* **2007**, *111*, 9600.

(32) NIST Standard Reference Database 69, NIST Chemistry WebBook. http://webbook.nist.gov/chemistry/ (June 2005 release).

(33) Turanyi, T.; Zalotai, L.; Dobe, S.; Berces, T. *Phys. Chem. Chem. Phys.* **2002**, *4*, 2568, and references therein.

(34) Luo, Y. R. *Handbook of Bond Energies (in Chinese)*; Science Press: Beijing, China, 2005.

(35) Bearpark, M. J.; Robb, M. A.; Schlegel, H. B. *Chem. Phys. Lett.* **1994**, *223*, 269.

(36) Salem, L. *Electrons in Chemical Reactions: First Principles*; Wiley: New York, 1982.

(37) Teller, E. *J. Phys. Chem.* **1937**, *41*, 109.

(38) Herzberg, G.; Longuet-Higgins, H. C. *Trans. Faraday Soc.* **1963**, *35*, 77.

(39) Gerhartz, W.; Poshusta, R. D.; Michl, J. *J. Am. Chem. Soc.* **1977**, *99*, 4263.

(40) Michl, J.; Bonacic-Koutecky, V. *Electronic Aspects of Organic Photochemistry*; Wiley: New York, 1990.

(41) Bonacic-Koutecky, V.; Koutecky, J.; Michl, J. *Angew. Chem., Int. Ed. Engl.* **1987**, *26*, 170.

(42) Su, H. M.; Bersohn, R. *J. Phys. Chem. A* **2001**, *105*, 9178.

(43) Zhao, H. M.; Bian, W. S.; Liu, K. *J. Phys. Chem. A* **2006**, *110*, 7858.

(44) Su, H. M.; Yang, J. X.; Ding, Y. H.; Feng, W. H.; Kong, F. A. *Chem. Phys. Lett.* **2000**, *326*, 73.

JP8075707